Microwave heating in heterogeneous catalysis
Modelling and design of rectangular traveling-wave microwave reactor

Yan, Peng; Stankiewicz, Andrzej I.; Eghbal Sarabi, Farnaz; Nigar, Hakan

DOI
10.1016/j.ces.2020.116383

Publication date
2021

Document Version
Final published version

Published in
Chemical Engineering Science

Chemical Engineering Science 232 (2021) 116383

Contents lists available at ScienceDirect

Chemical Engineering Science

journal homepage: www.elsevier.com/locate/ces

Microwave heating in heterogeneous catalysis: Modelling and design of rectangular traveling-wave microwave reactor

Peng Yan [a,b,1,*], Andrzej I. Stankiewicz [a], Farnaz Eghbal Sarabi [a], Hakan Nigar [a,*]

[a] Intensified Reaction & Separation Systems, Process & Energy Department, 3ME faculty, Delft University of Technology, Leeghwaterstraat 39, 2628 CB Delft, the Netherlands
[b] School of Chemical Engineering and Technology, Tianjin University, Tianjin 300072, China

HIGHLIGHTS

- The standard design procedure and characterization parameters of RTMR are proposed.
- The framework of multiphysics modeling for TMR is established.
- Novel RTMR is designed, optimized and evaluated regarding the heating performance.

ARTICLE INFO

Article history:
Received 11 June 2020
Received in revised form 1 October 2020
Accepted 11 December 2020
Available online 16 December 2020

Keywords:
Microwave reactor
Microwave heating
Microwave-assisted heterogeneous catalysis
Multiphysics modeling
Design and optimization
Process intensification

ABSTRACT

Microwave irradiation can intensify catalytic chemistry by selective and controlled microwave-catalytic packed-bed interaction. However, turning it to reality from laboratory to practical applications is hindered by challenges in the reactor design and scale-up. Here, we present a novel, rectangular traveling-wave microwave reactor (RTMR) and provide an easy-to-handle, 3-step design procedure of such reactor. The multiphysics model couples the electromagnetic field, heat transfer, and fluid dynamics in order to optimize the geometrical parameters and operational conditions for the microwave-assisted heterogeneous catalysis. The results show that the microwave energy input/output ports should be well-positioned and matched; otherwise, it would significantly decrease energy efficiency. In terms of microwave transmission, the RTMR presents a mix between the standing wave and the traveling-wave systems. Gas space velocity and input temperature significantly affect the temperature profile, and gas–solid temperature can present no significant difference under certain gas–solid contact.

1. Introduction

Microwave heating presents an interesting alternative to conventional conductive heating. It is very fast, selective, and volumetric in nature (Barham et al., 2019; Horikoshi and Serpone, 2014; Oliver Kappe, 2008; Stankiewicz, 2006; Stankiewicz et al., 2019). It can intensify catalytic reactions by enhanced product selectivity and higher conversion (Julian et al., 2019; Ramirez et al., 2019). In particular, microwave heating presents a tremendous opportunity in case of endothermic catalytic reactions, such as methane valorization processes. In microwave-assisted catalytic reactions, the catalyst and reactor designs play crucial role (Franssen et al., 2014). The key to success is a well-designed reactor with a microwave-responsive catalyst, which can utilize the microwave fields efficiently and in a controllable way.

Conventionally, mono-mode and multi-mode microwave reactors (Nigar et al., 2019; Stefanidis et al., 2014; Sturm et al., 2016) have some intrinsic drawbacks. In a mono-mode reactor, the heating performance is very sensitive to microwave frequency and the catalyst load position, and can only be applied to small heating volumes (Stankiewicz et al., 2019). These drawbacks can be seen in the reports from a Spainish (Julian et al., 2019) and a Japanese research group (Nishioka et al., 2013), where the available reactor volume is far smaller than the cavity volume and the microwave frequency must be tuned and controlled by an autonomous feedback control system to reach the resonance. In our research group the developed mono-mode reactor owns bulk tuners and reflectors to adjust the resonance frequency (Gangurde et al., 2017). A comprehensive understanding of the characteristics of the mono-mode reactor can be found in the study of Sturm et al. (Sturm et al., 2012, 2013). On the other hand, multi-mode reactors can operate with larger volumes, but their key intrinsic drawbacks are highly non-

* Corresponding authors.
E-mail addresses: yanpeng@tju.edu.cn (P. Yan), h.nigar@tudelft.nl (H. Nigar).
[1] Present address: Department of Chemical Engineering, Tsinghua University, Beijing 100084, China.

https://doi.org/10.1016/j.ces.2020.116383
0009-2509/

Nomenclature

Roman letters

A	surface area (m^2)
C_p	heat capacity (J/kg/K)
E	electric field vector (V/m)
E*	complex conjugate of **E** (V/m)
E	normalized electric field intensity (V/m)
f	frequency (Hz)
h_{sf}	coefficient of fluid–solid interphase heat transfer (W/m^2/K)
k	thermal conductivity (W/m/K)
k_o	wavenumber (−)
K	bed permeability (m^2)
L	the characteristic length (m)
P	microwave energy (W)
p	pressure (Pa)
Pr	Prandtl number
Re	Reynolds Number
Nu	Nusselt number
SWR	standing wave ratio
T	temperature (°C)
t	time (s)
TE	transverse electric mode
TEM	transverse electromagnetic mode
u	flow velocity vector field for the ×, y, z directions
Q_{MW}	volumetric microwave power dissipation (W/m^3)
Q_s	heat source term, standing for the heat loss to the environment (W/m^3)

Greek letters

β_F	Forchheimer drag coefficient (kg/m^4)
C_f	friction coefficient (−)
ε	permittivity (F/m)
ε_0	permittivity of free space (F/m)
ε_r	relative permittivity (−)
ε'_r	relative dielectric constant (−)
ε_r''	relative dielectric loss factor (−)
μ	permeability (H/m)
μ_r	relative permeability (−)
η	energy efficiency (−)
←	electrical conductivity (S/m)
γ	viscosity (Pa·s)
ρ	density (kg/m^3)
ω	angular frequency (rad/s)
θ	volume fraction

Subscripts

s	solid phase
g	gas phase
max	maximum value
min	minimum value
MWin	microwave energy input
eff	effective
loss	energy loss
trans	transmission
ref	reflection

Note

- The variables in bold fonts represent the vector fields.

uniform heating and poor temperature controllability (Stankiewicz et al., 2019; Sturm et al., 2016). These disadvantages can be seen from the research reported by Gao et al. (Gao et al., 2019) where the large volume indeed is accompanied by non-uniform heating and poor controllability. Here just name a few, for more details and discussion, interested readers can refer to the book chapter by Sturm et al. (Sturm et al., 2016) and the review paper (Stankiewicz et al., 2019).

To avoid the inherent disadvantages for catalytic applications in current resonant cavity type of microwave reactors, a novel reactor concept based on the traveling-wave principle has been proposed by Sturm (Sturm et al., 2014), where the feasibility of this concept and the merit of homogeneous heating are proved by adopting liquid water as the medium in monolithic reactor structure, and further developed and investigated by Eghbal Sarabi et al. (Eghbal Sarabi et al., 2020) for heterogeneous gas–solid catalysis process. Similarly, traveling-wave concept is also reflected in the research reported by Polaert et al. (Polaert et al., 2017) and Mitani et al. (Mitani et al., 2016). They adopted traveling-wave concept to conduct aqueous process or reaction, and both of the results indicate its advantages of larger volume and better temperature controllability. Furthermore, Muley et al. conduct biomass pyrolysis in a rectangular traveling-wave microwave reactor concept and present a better energy utilization (Muley et al., 2016). The results of those studies show some clear advantages of the traveling-wave reactor systems: larger volume, less sensitive to microwave frequency, and better temperature controllability and uniformity, however rare research is reported for heterogeneous gas–solid catalysis. Therefore, more endeavors are needed to obtain fundamental understanding and advance them to the higher Technology Readiness Levels (TRL). Amongst, designing novel and robust traveling-wave microwave reactor, developing general modeling methodology and obtaining deep insights in microwave heating behavior are urgently needed.

The microwave reactor design is a highly inter-disciplinary job, because it involves microwave physics, electrical engineering, materials science, and chemical engineering (Eghbal Sarabi et al., 2020; Stankiewicz, 2006). Therefore, development of a standard design procedure is highly desired for chemical engineer who focus on heterogeneous catalysis and know less about microwave reactor. Unfortunately, there are no such design guidelines for microwave reactors available in literature, especially for traveling-wave microwave reactors.

Obviously, in chemical reactor design modeling plays a crucial role. However, the multiphysics models of microwave reactors are extremely scarce, and in particular no robust model has been reported so far for the traveling-wave microwave reactors.

In the current paper, a novel traveling-wave microwave reactor is designed, modeled, and evaluated. The standard design procedure for travelling-wave microwave reactor is proposed and thus a novel RTMR is designed in Section 2; meanwhile the performance parameters characterizing the travelling-wave microwave reactor are recommended. A coupled multiphysics reactor model involving microwave field, fluid flow, and heat transfer with emphasis on local thermal non-equilibrium is established with the focus on heat management in Section 3. Based on the above design procedure and multiphysics model, the reactor performance is studied aiming

at the optimization of its geometry and operational conditions as discussed in Section 4.

2. RTMR design and characterization

2.1. Standard design procedure

Fig. 1 presents a three-step procedure to design a robust Rectangular Traveling-Wave Microwave Reactor. The rules and reasons for each step are presented in detail below.

2.1.1. Step 1: Waveguide selection

The electromagnetic field modes and wave propagation are determined by the geometry and dimensions of transmission line, e.g., coaxial, and waveguides, i.e., rectangular and circular (Pozar, 2012a). The coaxial transmission line reactor concept has already been investigated by Eghbal Sarabi *et al.* (Eghbal Sarabi et al., 2020). On the other hand, rectangular waveguide can also be used in the traveling-wave concept. Above a certain frequency, the so-called cutoff frequency ($f_{c_{mn}}$), the electromagnetic waves propagate inside the waveguide. For a rectangular cross-section (see Fig. 2), the cutoff frequency can be calculated with the following equation:

$$f_{cmn} = \frac{1}{2\pi\sqrt{\mu\varepsilon}}\sqrt{\left(\frac{m}{a}\pi\right)^2 + \left(\frac{n}{b}\pi\right)^2} \quad (1)$$

Each combination of m and n are known as mode and each of them has a cutoff frequency. For example TE_{10}: m:1 and n:0 so here m and n indicate the number of variations in the electromagnetic wave pattern in the × and y directions, respectively. Since there is no TE_{00}, the dominant mode in this rectangular type is TE_{10} (Pozar, 2012b). In the TE mode, electric field vectors in the cavity are perpendicular, i.e., transverse, to the z-direction, which is the direction of the propagation.

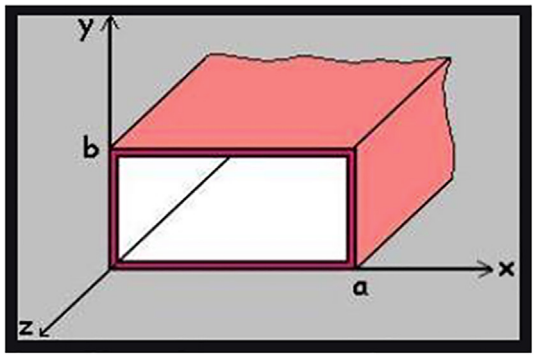

Fig. 2. The rectangular waveguide in the Cartesian coordinate system.

Here, considering the significant advantages of industrial standard (ease of fabrication) and high power-handling over coaxial transmission line, we chose the standard rectangular cross-section waveguide named WR-340 (86.4 mm in width and 43.2 mm in height) as the starting point for the design. The sinusoidal electric field distribution at the cross-section is depicted in Fig. 3.

2.1.2. Step 2: Coaxial cable-to-waveguide connection and its optimization

Safe transmission of microwave power through the waveguide is critical for the operation of a microwave reactor. The standard cable to connect solid-state microwave generator is a coaxial cable that transfers microwave energy in the Transverse Electromagnetic (TEM) mode. Generally, the power connections can be allocated to different surfaces and then presents various matches for the microwave energy input/output ports.

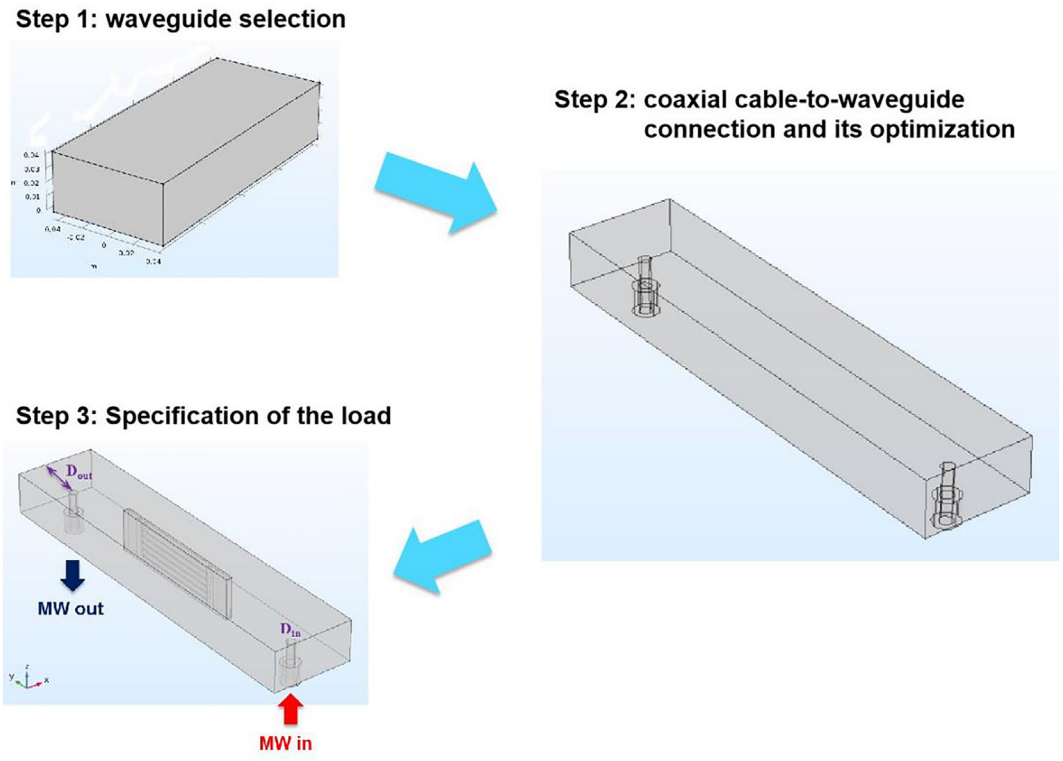

Fig. 1. The proposed standard procedure for RTMR design.

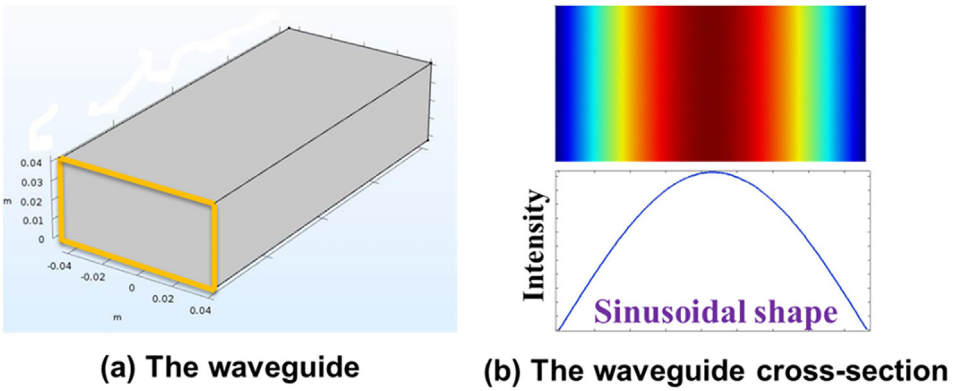

Fig. 3. The WR-340 waveguide and its electric field distribution at the cross-section.

2.1.3. Step 3. Specification of the load

Positioning of the load is important for taking full advantage of the microwave field distribution. Given the sinusoidal distribution of the electric field inside the rectangular waveguide, we decide to design a rectangular fixed bed and locate it at the center where the highest intensity of the electric field presents, see Fig. 3b. In this way, the interaction between the load and microwaves will be maximum. Here, the specific design of the load is shown in Fig. 4. The catalyst load that consists of 6 channels is positioned in the middle between two inert layers of porous quartz particles. The quartz particle layers, transparent to microwave, are used to support the catalyst bed and distribute the gas.

Moreover, the different positions of coaxial connectors and their match besides the above-mentioned allocated surface significantly affect both the microwave field distribution and the energy dissipation inside the waveguide. Therefore, further optimization combined with the load is quite necessary.

2.2. Characteristics and performance parameters

The performance evaluation of a microwave reactor is very different from that in a conventional reactor. The key parameters for evaluating the performance of a microwave reactor are related to the energy balance and field intensity in the device.

2.2.1. Energy balance

Energy balance is the fundamental tool to assess the energetic efficiency of a microwave system (Bermúdez et al., 2015). Since the traveling-wave microwave reactor is an open system with an energy input port and energy output port, the energy balance of the traveling-wave microwave reactor is different from the standing-wave reactor (semi-open system for multi-mode and mono-mode cavity), as shown in Eq. (2). From the equation, we can see that the total microwave energy input contains not only the effective energy and the energy loss but also comprises the transmitted energy out of the TMR output port, the reflection out of the TMR through the input port. For the standing-wave reactor, the system is semi-open with only one energy port. The total energy input can be divided into 3 parts, namely the effective part dissipated inside the catalytic bed, the energy loss on cavity walls, and the reflected energy, as shown in Eq. (3). The clear difference in energy balance between standing-wave and traveling-wave microwave reactors can be viewed in the Equations (2, 3). The energy efficiency, η, is defined by Eq. (4) to indicate how much energy is available to heterogeneous catalysis.

$$P_{MWin} = P_{eff} + P_{loss} + P_{ref} + P_{trans} \tag{2}$$

$$P_{MWin} = P_{eff} + P_{loss} + P_{ref} \tag{3}$$

$$\eta = P_{eff}/P_{MWin} \tag{4}$$

where P_{MWin} represents the total energy input to the reactor by microwave heating; P_{eff}, P_{loss} are the effective dissipation into the catalytic bed, and the energy loss on the waveguide walls due to the wall electric current, respectively; P_{trans}, P_{ref} are the energy part of transmitting out of the microwave reactor by the output port and the energy reflected by the loading out of the input port.

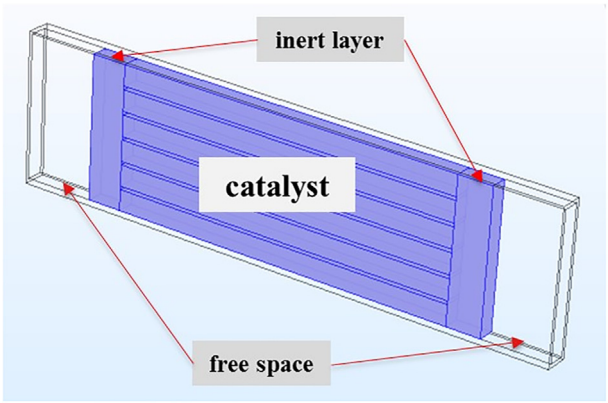

Fig. 4. The designed load in the RTMR.

2.2.2. Standing wave ratio

A perfect traveling microwave presents a gradual decrease in time-averaged electric field intensity and zero reflection when passing through the media. However, solid media are not entirely transparent to microwaves and also the length of the solid load is limited, which inevitably produces at least two interface (Sturm et al., 2013). In current design, different mediums produce two gas–solid media interfaces at the beginning and the ending, where it produces multiple reflections of microwaves inside the media. See Fig. 4 (free space: gas and catalyst: microwave absorbing media). Due to the inner reflections, a standing-wave pattern is generated; therefore, the wave propagation inside the traveling-wave microwave reactor is not entirely traveling-wave anymore. As a result, the time-averaged electric field intensity will not be absolutely monotonic decrease and presents wavy fluctuation instead (Pozar, 2012b; Sturm et al., 2014).

In the resonant microwave cavities (mono- and multi-modes), microwave travels forth and back and forms a resonant standing-wave pattern where the electric and magnetic energy is stored (Pozar, 2012b; Sturm et al., 2014). In the designed travelling-

wave microwave reactor, the microwave is reflected back and forth by the gas–solid media interfaces inside the solid region until the microwave is totally dissipated. In other words, the electric field pattern inside the solid media consists of both traveling-wave microwave component and standing-wave microwave component. The intensity of the standing-wave microwave component can be described by the standing wave ratio (SWR), defined by Eq.(5), which can be preliminarily used to electric field profile along propagation direction. The smaller SWR is, the flat/uniform electric field profile will be.

$$SWR = \frac{E_{\max}}{E_{\min}} \tag{5}$$

where E_{max} and E_{min} represent the maximum and minimum of normalized electric field intensity inside the solid media. Accordingly, SWR = ∞ for the perfect standing wave ratio and SWR = 1 for the perfect traveling-wave microwave.

3. Mathematical model of multiphysics coupling

A three-dimensional mathematical model is developed using COMSOL Multiphysics® simulation environment. The model fully couples electromagnetic waves, heat transfer, and fluid dynamics. The steady-state simulation is conducted, and the frequency domain analysis is used for the electromagnetic field.

As for the coupling of multiple physics module, electromagnetic field and heat transfer are coupled by the source term of microwave heating, fluid dynamics is coupled with heat transfer by providing velocity field for heat transfer equations to calculate temperature distribution, and most of physical properties in electromagnetic field and fluid dynamics are temperature-dependent and thus associated with heat transfer module. Because the effect of electromagnetic field from the other field is relatively weak, the electromagnetic field is first solved and then supply initial values for heat transfer and fluid dynamics. Fully coupled velocity, pressure, temperature are solved simultaneously by re-configure the solver to be a segregate. Finally, two segregates (one is the electromagnetic field variable, the other is the variables of fluid dynamics and heat transfer) are solved in sequence and iterated until final convergence.

The following sections demonstrate the governing equations and boundary conditions for all the physic modules applied.

3.1. Electromagnetic field

The electromagnetic field distribution and the volumetric heat generation in the packed bed are calculated by solving the following equations.

$$\nabla \times \mu_r^{-1}(\nabla \times \boldsymbol{E}) - k_0^2(\varepsilon_r - j\frac{\sigma}{\omega\varepsilon_0})\boldsymbol{E} = 0 \tag{6}$$

$$Q_{MW} = \omega\varepsilon_0\varepsilon_r''\boldsymbol{E}\cdot\boldsymbol{E}^* \tag{7}$$

where **E** (V/m) is the electric field vector, **E*** is the complex conjugate of **E**, $\omega = 2\pi f$ (rad/s) is the angular frequency, ε_r, μ_r stands for the relative permittivity and permeability of the media, ε_0 is the absolute permittivity of vacuum space,$\varepsilon_r', \varepsilon_r''$ are the dielectric constant and dielectric loss respectively, namely the real part and imaginary part of relative permittivity, ←is the electrical conductivity of the media, $k_o = 2\pi/\lambda$ is the wavenumber. The *Electromagnetic waves, Frequency Domain* module in COMSOL Multiphysics software is used for solving the equations (COMSOL, 2017c).

The electromagnetic properties of the porous media are calculated based on the volume average assumption, as shown in Eqs. (8)–(10):

$$\mu_r = \theta_s\mu_{r,s} + (1-\theta_s)\mu_{r,g} \tag{8}$$

$$\varepsilon_r = \theta_s\varepsilon_{r,s} + (1-\theta_s)\varepsilon_{r,g} \tag{9}$$

$$\sigma_r = \theta_s\sigma_{r,s} + (1-\theta_s)\sigma_{r,g} \tag{10}$$

where subscripts s and g represent solid phase and gas phase respectively, and θ stands for the volume fraction of the phase in the physical domain.

The above equations are solved in the microwave heating region, including the quartz tube, the catalyst bed, the air domain between the quartz tube and the waveguide inner wall.

3.2. Heat transfer

The heat transfer module is applied in all the domains (catalyst bed, air, quartz tube, waveguide inner wall, etc.) since both the microwave heating domain and the other domains are involved in the microwave heating, heat conduction or convective heat transfer (COMSOL, 2017b). The *Heat Transfer Module* in COMSOL Multiphysics is used for the solution.

For microwave heating in heterogeneous catalysis, local hot spots can be frequently generated at the catalyst particle surface or vicinal contact point as a results of differential heating (Haneishi et al., 2019; Horikoshi and Serpone, 2014), which is of significant importance to obtain micro-scale insights. However, herein our goal is to obtain macro-scale insights of microwave heating from the view of whole reactor. The absence of hot spots is assumed and the homogenization method as Eq. (11) and (14) is adopted.

3.2.1. Local thermal equilibrium

Usually, the heat transfer with microwave heating in the fixed bed is modeled assuming the local thermal equilibrium between gas and solid phase in the porous medium. To this end, Equations (11–13) are usually applied. In Equation (11), the first term on the left-hand side is the rate of heat accumulation, and the second and third terms are convective and conductive contributions. On the right-hand side, the first term, Q_{MW}, is the volumetric power dissipation (see Equation (7)) of microwave irradiation, which was calculated from the electromagnetic field distribution, and the second term, Q_s, stands for the heat loss to the environment by the quartz reactor walls.

$$(\rho C_P)_{eff}\frac{\partial T}{\partial t} + \rho_f C_{P,f}\boldsymbol{u_f}\cdot\nabla T - k_{eff}\nabla T = Q_{MW} + Q_s \tag{11}$$

$$(\rho C_P)_{eff} = \theta_s\rho_s C_{P,s} + (1-\theta_f)\rho_f C_{P,f} \tag{12}$$

$$k_{eff} = \theta_s k_s + (1-\theta_s)k_f \tag{13}$$

Further, in the above equations ρ, C_p, k are the density, heat capacity and thermal conductivity, respectively; $\boldsymbol{u_f}$ stands for the flow velocity field, T is the local temperature of the calculated domain; $(\rho C_p)_{eff}$, k_{eff} are the effective volumetric heat capacity at constant pressure and effective thermal conductivity, respectively. The subscripts, s, f, represent the solid phase and fluid phase respectively and θ means the volume fraction for each phase.

3.2.2. Local thermal non-equilibrium

Microwave heating is selective and volumetric, and the solid phase temperature is usually heated faster than the gas phase. Hence, the local thermal equilibrium (LTE) assumption is not valid anymore. Here, we propose to use the local thermal non-equilibrium (LTNE) approach, in order to solve temperature fields in both gas and solid phase. Three main points of the LTNE approach are as follows:

i. The "local" term indicates to the pointwise comparison of the temperatures of solid and gas. Two different equations, Equations (14, 15), are used to describe the heat transfer for the solid phase and gas phase, respectively.
ii. The interphase heat transfer is calculated by adopting the fluid–solid heat transfer coefficient in Eq. (16) (Wakao, 1976; Wakao et al., 1979).
iii. The gas phase is assumed to be 100% microwave transparent and the microwave heating source term is only available to the solid phase.

Solid phase:

$$\rho_s C_{P,s}\frac{\partial T}{\partial t} + \theta_s \rho_S C_{p,S}\boldsymbol{u_s}\cdot\nabla T_s + \nabla\cdot[-\theta_s k_s \nabla T_s] = Q_{MW} + h_{sf}A(T_f - T_s) + Q_s \quad (14)$$

Gas phase:

$$\rho_s C_{P,s}\frac{\partial T}{\partial t} + (1-\theta_s)\rho_f C_{p,f}\boldsymbol{u_f}\cdot\nabla T_f + \nabla\cdot[-(1-\theta_s)k_f\nabla T_f] = h_{sf}A(T_s - T_f) + Q_s \quad (15)$$

Wakao's equation:

$$\frac{h_{sf}L}{k_s} = Nu = 2.0 + 1.1\mathrm{Pr}^{1/3}Re_p^{0.6} \quad (16)$$

In Equations (14–16), ρ, C_p, k are the density, heat capacity and thermal conductivity, respectively. **u** stands for the flow velocity field; T is the local temperature of the calculated domain. A, h_{sf} represents the surface area and the coefficient of fluid–solid interphase heat transfer, and *s, f* in the equations are generally solid phase, fluid phase. The characteristic length, L, is the particle diameter of the packed bed. Nu, Pr, Re_p stands for the Nusselt number, Prandtl number, and Reynolds number of the particle-based packed bed, respectively.

3.3. Fluid dynamics

The fluid dynamics in the packed bed are represented by time-dependent incompressible fluid flow according to Eqs. (17)–(21). The equations are only solved in the porous media domain where the fluid flows through the packed bed. The *Laminar Flow* module with the setting of porous media is used (COMSOL, 2017a).

Momentum transfer equation:

$$\frac{\rho}{1-\theta_s}\frac{\partial \boldsymbol{u_f}}{\partial t} + \frac{\rho}{1-\theta_s}(\boldsymbol{u_f}\cdot\nabla)\boldsymbol{u_f}\frac{1}{1-\theta_s} = \nabla\cdot\left[-P + \frac{\gamma}{1-\theta_s}(\nabla\boldsymbol{u_f} + (\nabla\boldsymbol{u_f})^T) - \frac{2}{3}\frac{\gamma}{1-\theta_s}\nabla\cdot\boldsymbol{u_f}\right] - \left(\frac{\gamma}{K} + \beta_F|\boldsymbol{u_f}|\right)\boldsymbol{u_f} \quad (17)$$

where

$$K = \frac{(1-\theta_s)^3 d_p^2}{150\cdot\theta_s^2} \quad (18)$$

$$\beta_F = \frac{\rho_f(1-\theta_s)C_f}{\sqrt{K}} \quad (19)$$

$$C_f = \frac{1.75}{\sqrt{150(1-\theta_s)^3}} \quad (20)$$

Continuity equation:

$$\nabla\cdot(\rho\boldsymbol{u_f}) = 0 \quad (21)$$

In the momentum transfer equation, the first and second terms on the left side represent accumulation term and convective flow term, respectively. On the right side, there are pressure gradient, viscous forces, and the additional term (Bird et al., 2002). The additional term comes from *Brinkman-Forchheimer* equation, and this term takes into account all drag contributions to the fluid flow exerted by the porous media (Nield and Bejan, 2017). K, β_F, C_f, γ, d_p represent the permeability of porous media, the Forchheimer drag coefficient, friction coefficient, gas viscosity and catalyst particle dimension, respectively.

3.4. Boundary conditions

For the electromagnetic field, the following boundary conditions are set:

i. The microwave frequency is specified as 2.45 GHz and the waveguide walls are defined as copper with impedance boundary condition this is to account for the electric surface current present in the metallic walls.
ii. The "microwave in" and "microwave out" ports (see Fig. 1) are coaxial in and out connectors. Hence, the type of the ports has been assigned as TEM mode. Only the "microwave in" port has been excited with a power of 100 W.

In order to simplify the modeling and simulation of the designed TMR, several assumptions on boundary conditions for heat transfer and fluid dynamics are made as follows:

i. The heat loss by the porous packed bed to the environment is calculated by heat transfer coefficient of 10 $W/m^2/K$ through the quartz wall.
ii. The air domain between porous packed bed and waveguide is obviously above the ambient temperature. In view of the aimed reaction of methane valorization, the constant temperature 573.15 K is assumed.
iii. There are multiple adjacent domains in the RTMR model, so several interfaces come into existence. Considering the simplification and reliability, all the interfaces are assigned as continuous in temperature, namely $T_a = T_b$.

For parametric analysis, the flow input is assumed as a fully developed laminar flow with space velocities varying between 0.135 and 0.54 m/s, and temperatures varying between 297.15 K and 897.15 K. The boundary conditions at the flow output are zero heat flux and ambient pressure. Also, the no-slip condition is applied for fluid flow in porous packed-bed.

3.5. Materials properties and packed bed parameters

The materials properties and the parameters of the porous packed bed are presented in Tables 1 and 2, respectively.

4. Results and discussion

Three ways can be adopted to control the microwave energy utilization and temperature distribution in the RTMR:

Table 1
Materials used in the model and their properties.

	Relative permittivity	Relative permeability	Electric conductivity(S/m)	Density(kg/m^3)	Heat capacity (kJ/kg/K)	Thermal conductivity(W/m/K)
Copper	1	1	Default	Default	Default	400
Quartz	3.8–0.00038i[a]	1	$1 * 10^{-12}$	2600	820	3
Zeolite[b]	3.27–0.57i	1	0	800	0.836	0.15
Air	1	1	0	Default	Default	Default
Dielectrics of coaxial connector[c]	2	1	0	–	–	–

Notes: *Default* means that the built-in database is used and the physical quantity is temperature-dependent, see the details in *Table S1*.
"-" means that the physical quantity is not needed.
a. The data is cited from (Nigar et al., 2019).
b The data is cited from (Nigar et al., 2015; Nigar et al., 2019; Satterfield, 1996).
c The dielectrics of coaxial connector is Teflon, and assume it zero dielectric loss here considering its extremely low loss factor.

Table 2
The parameters of porous packed-bed.

Parameter	Dimension
Shape	sphere
Diameter	1 mm
Porosity	0.4
Specific surface area	3140 m^2/m^3

i. Manipulate the microwave field distribution by the reactor configuration design, such as the optimization of microwave energy ports' positions;
ii. Manipulate the load position and geometry of packed bed as discussed in Section 2;
iii. Manipulate the operating conditions, which is the most convenient and important way in industry, such as the fluid temperature and the fluid velocity of the reactants.

4.1. Optimization of microwave energy input/output ports' position

According to our proposed standard design procedure for TMR, preliminary screening regarding the port position, which surface of the waveguide, need to be done. Our research indicates that the reflected energy is too high when the configuration of the input and output port are either on the different waveguide surface or simultaneously on the side or the end surface of waveguide. Correspondingly, the reflected energy is negligible when the ports are on the upper/lower surface. Therefore, this preliminary configuration is selected for the further optimization of microwave energy ports coupled with catalytic bed as depicted in Step 3. The optimization in step 3 is highlighted below.

As for the coupled optimization as depicted in step 3, Fig. 5 shows the vertical connection of the coaxial cable to the rectangular waveguide, which shifts TEM mode to Transverse Electric, TE_{10} mode, smoothly. Two key parameters, the distance between the coaxial port and the waveguide wall (D_{in}, D_{out}), influence the microwave energy transmission significantly. According to the fundamentals of microwave engineering (Pozar, 2012b), it is recommended that that distance is one-quarter of vacuum wavelength (30.5 mm) or waveguide wavelength (43.2 mm). Here, we additionally adopt two more values (37 mm, 43.59 mm) to perform the sensitivity study to prove how sensitive to minor change the microwave travelling is. This leads to 16 variants of configuration as shown in Table 3.

In the traveling-wave microwave reactor, the input microwave power is divided into four components, namely: (i) the effective dissipation, (ii) the loss in waveguide walls, (iii) the transmission via the outlet port, and (iv) the reflection. Fig. 6 presents the effect of microwave energy ports positions on energy distribution and it is obvious that the energy distribution is sensitive to the energy ports position. The results indicate that the group of D_{in} = 30.5 mm and D_{out} = 30.5 mm is the best configuration, which shows the

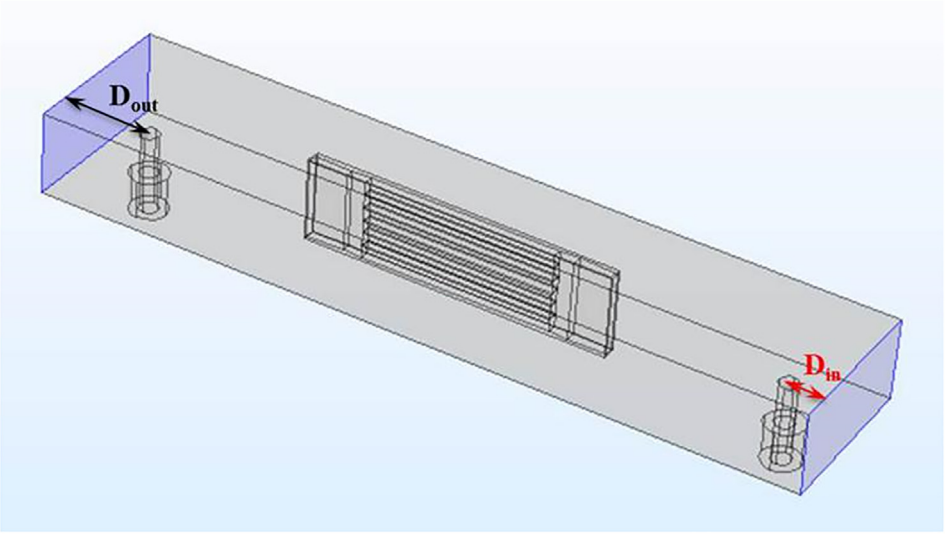

Fig. 5. The proposed configuration of traveling microwave with emphasis on microwave energy input/output ports' positions.

Table 3
The proposed configurations of microwave ports position.

Configuration No.	D_{in}/mm	D_{out}/mm
1	30.5	30.5
2	30.5	37
3	30.5	43.2
4	30.5	43.59
5	37	30.5
6	37	37
7	37	43.2
8	37	43.59
9	43.2	30.5
10	43.2	37
11	43.2	43.2
12	43.2	43.59
13	43.59	30.5
14	43.59	37
15	43.59	43.2
16	43.59	43.59

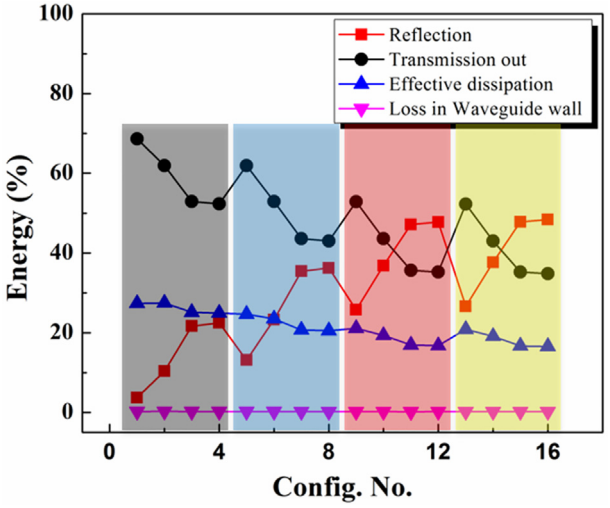

Fig. 6. The effect of microwave energy ports configurations on energy distribution.

highest percentage in effective dissipation (27.5%), the least reflection energy (3.6%) and the highest percentage in transmission via the outlet port which can be further utilized (Stankiewicz et al., 2019) and finally its energy efficiency is 27.5%. Comparing all the configurations, particularly config. 1, 6, 11, 16, we can find that the reflection is extreme sensitive to the port position and it can vary from 3.6% to almost 50%. It can also be seen that the distance to the end wall should be closer to one-quarter of vacuum wavelength other than waveguide wavelength for either input port or output port. Plus, the bigger deviation results in higher reflection. More attention in further research should be paid to weaken the reflection because the reflected energy is unavailable to the catalytic bed and even harmful to microwave generator.

The study in the following sections are based on the optimized ports' configuration (D_{in} = D_{out} = 30.5 mm).

4.2. Microwave transmission characteristics in the RTMR

Fig. 7 depicts the overall electric field distribution along the reactor. Two extreme peaks can be observed at the microwave input port and output port because the microwave mode shifts from TEM to TE_{10}. In the region of the packed bed, the overall trend of electric field intensity decreases along with the wavy fluctuation. The wavy fluctuation with the obvious peaks originates from the mix of standing-wave and traveling wave. The imperfection of traveling wave is expressed by the standing wave ratio (SWR) and the value is 1.73 (see Section 2.2.2 for thorough understanding).

$$SWR = \frac{E_{max}}{E_{min}} = 1.73$$

4.3. Temperature distribution in the packed bed without fluid flow

Fig. 8 represents the temperature distribution in the packed bed under zero gas velocity with a 100 W microwave power input. The catalyst bed exhibits two high-temperature peaks which are identical to the distribution of electric field intensity. It implies that the microwave heating rate is much higher than the heat conduction in current catalytic bed. Also, the central temperature for each channel is always higher than that at the edges, which can be seen from the transverse temperature profile in Fig. S1. In view of the temperature distribution at all directions, in order to achieve more uniform (flat) temperature profile, more intense heat conduction of catalytic bed which is comparable to microwave heating rate is preferable.

4.4. Temperature distribution in the packed bed with fluid flow

Generally, operational conditions significantly affect the temperature distribution of the packed bed. Fig. 9 depicts the temperature distribution of the catalyst bed with the effect of fluid flow. Compared to Fig. 8 where two distinct temperature peaks exists, it is clear that the fluid flow almost make the first temperature peak disappear and pushes the second temperature peak back and smoothes the temperature profile to some extent. This is attributed to the heat transfer behavior from hot catalytic bed to cold flowing gas.

Also, the results indicate that the temperature of gas phase and solid phase are almost the same although the local thermal non-equilibrium approach is adopted. This is different from that reported by Julian et al. in which they observed a significant temperature difference between gas and solid phase in monolithic catalyst (Julian et al., 2019). We deduce that this phenomenon is attributed to faster heat transfer in particle-based catalytic bed in comparison with that in monolithic bed since the particle-based catalytic bed herein owns higher specific surface area (3140 m^2/m^3 in this study vs. 2740 m^2/m^3 for monolithic bed) and the gas turbulence can be formed (in contrast, laminar flow in monolithic bed). The above speculation is also supported by the experiments recently reported by Ramirez et al., where they compared gas–solid temperature difference between foam-based bed and monolithic bed and find that higher gas–solid contact weakens the gas–solid temperature difference (Ramirez et al., 2020).

Fig. 10 shows the effect of gas temperature on the temperature profile in the packed bed. It is obvious that lower gas temperature generates less uniform temperature profile and the temperature deviates the average temperature much more. But too low inlet gas temperature, for instance 297.15 K, will definitely quench part of the packed bed, it leads to dramatically decreasing catalytic region available and efficient for activating the catalytic reaction because the catalytic reactions need to be activated above certain a temperature and more efficient in small temperature range. In order to achieve a flat temperature profile which is the most desirable for the catalytic reactor, higher input gas temperature, particularly closing to the average temperature of the packed bed, is highly desired. Therefore, the preheating of the gas in the RTMR is recommended as used in the conventional heated reactor.

Fig. 11 shows the effect of gas velocity on temperature profile in the packed bed. It can be observed that higher gas velocity brings

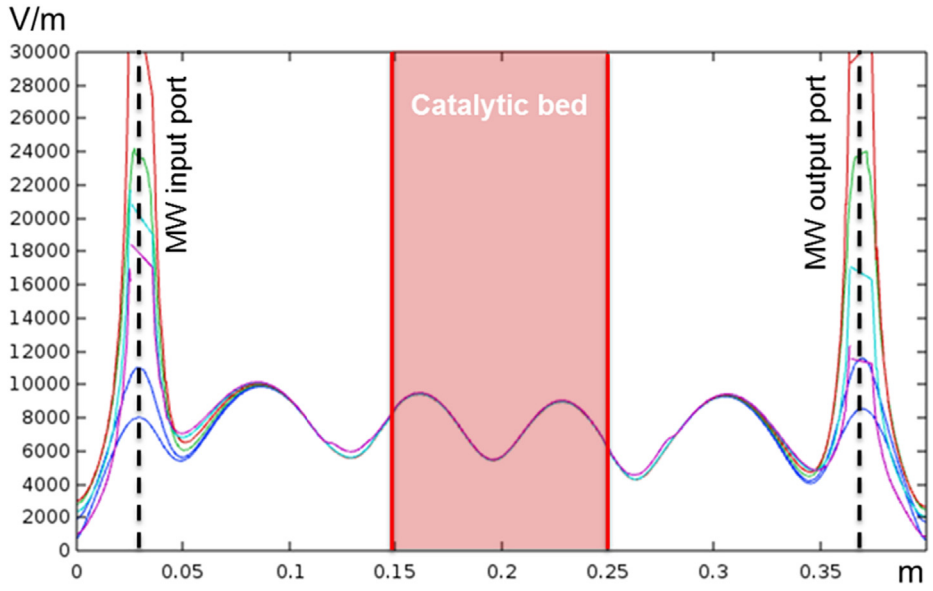

Fig. 7. Normalized electric field intensity distribution along the reactor. Data lines represent 6 sampling positions along the centerline of each channel in the packed bed.

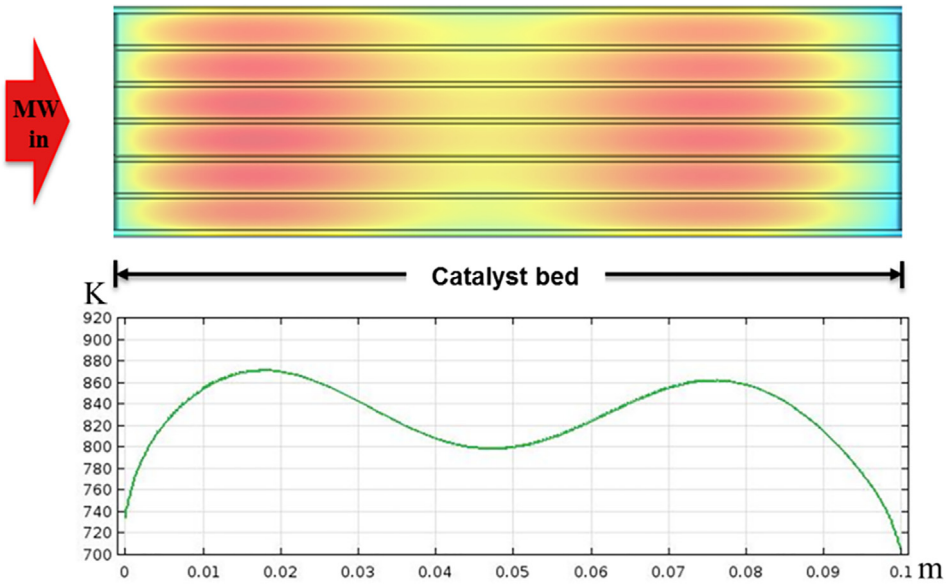

Fig. 8. Temperature distribution without fluid flow in the packed bed. (a) Central cross-section, (b) the average temperature of the central cross-section.

about the steep temperature profile, and the deviation from average value can reach up to 35%. Obviously, higher temperature gradient in the reactor shrinks the efficient region for catalytic reactions, which reminds us that a lower gas flow rate is preferable in terms of obtaining the flat temperature profile. However, higher gas velocity can produces high process throughput, in this way we should weigh the importance between the throughput and the efficient catalytic region and find the balance to maximize the process throughput per RTMR reactor volume.

5. Conclusions

In this study, we have introduced a 3-step standard procedure for designing a novel rectangular traveling-wave microwave reactor with fixed bed of catalyst and point out the microwave propagation features in the RTMR. We build the mathematical model which successfully couple electromagnetic field, heat transfer and fluid dynamics in COMSOL Multiphysics simulation environment. Based on the multiphysics model the structural and operational optimization has been studied. From the performed research the following conclusions can be drawn:

i. The microwave propagation inside the RTWR is the mix of ideal traveling-wave and ideal standing-wave, the extent of which can be described by the standing-wave ratio. In this case, it is 1.73 and higher deviation from one indicates more component of standing wave that is unwanted.

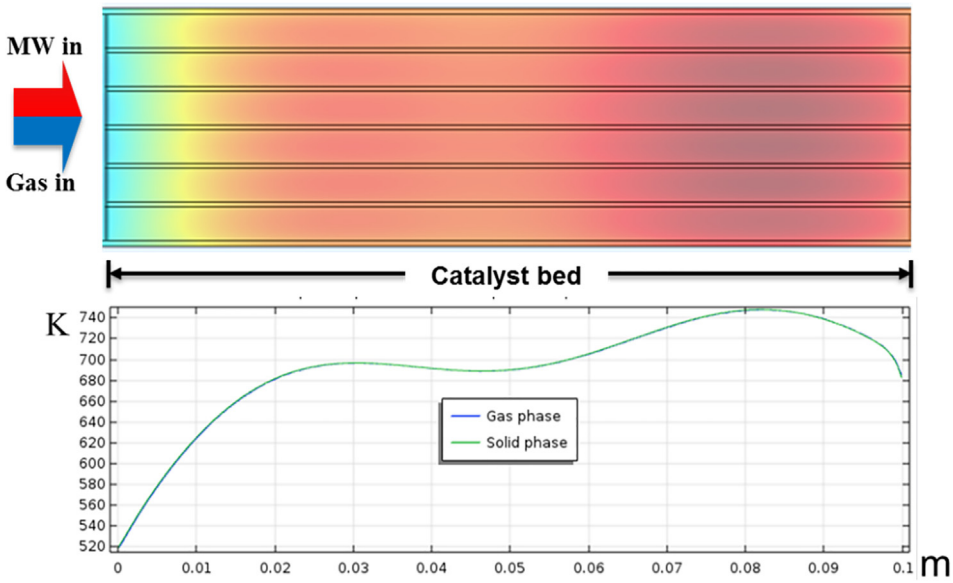

Fig. 9. Temperature distribution in presence of fluid flow in the packed bed (gas temperature: 297.15 K, gas velocity: 0.135 m/s). (a) central cross-section, (b) the average temperature of the central cross-section for both gas phase and solid phase.

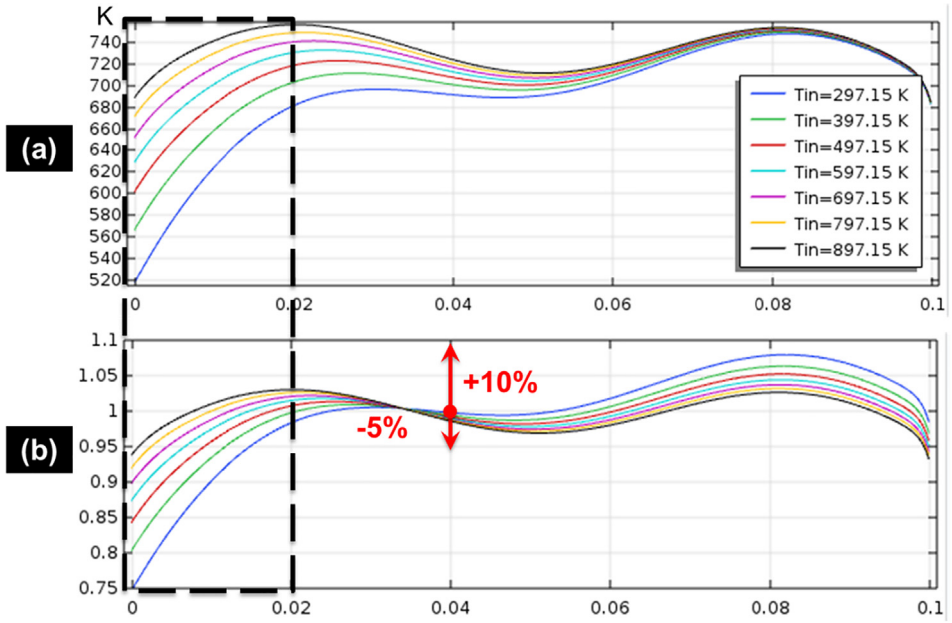

Fig. 10. The effect of gas temperature on temperature profile in the packed bed under the gas velocity of 0.135 m/s. (a) the temperature profile, (b) the relative deviation from average temperature.

ii. The positions of microwave energy input/output ports matter and affect the energy allocation in the whole RTWR system. The best configuration is D_{in} = D_{out} = 30.5 mm and in this case the highest energy efficiency (effective dissipation 27.5%) and lowest reflection (3.6%) are achieved.

iii. The temperature profile in the axial direction is wavy in absence of the gas flow. It proves that the microwave heating rate is far higher than the heat conducting ability of the porous packed bed and the more conductive bed should be used for a smooth temperature profile.

iv. There is no obvious difference between gas and solid temperatures although the local thermal non-equilibrium approach is adopted, so whether there is significant discrepancy between gas and solid temperature really depends: more gas–solid contact in the catalytic bed (i.e. turbulence, high specific surface area etc.) decreases gas–solid temperature difference.

v. The operational conditions (gas temperature and velocity) affect the axial temperature profile tremendously. The maximum deviation (circa 35%) from averaged temperature occurs at the lowest gas temperature (297.15 K as studied) and the highest gas velocity (0.54 m/s as studied). This imply

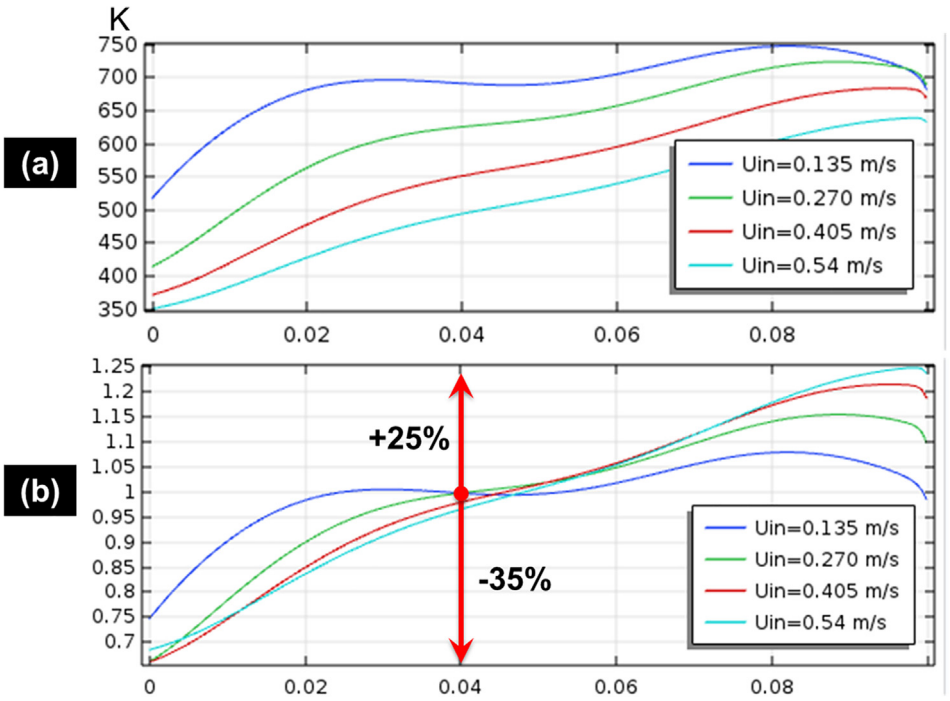

Fig. 11. The effect of gas velocity on temperature profile in the packed bed under the gas temperature of 297.15 K. (a) the temperature profile, (b) the relative deviation from average temperature.

that both gas pre-heating and gas velocity should be well considered in order to maximize the energy efficiency and process throughput per reactor volume.

All in all, this paper provides fundamental insights in the development of traveling-wave microwave reactors and paves the way for bridging the gap between microwave chemistry and industrial practice.

CRediT authorship contribution statement

Peng Yan: Conceptualization, Investigation, Validation, Software, Writing - original draft, Writing - review & editing, Funding acquisation (CSC scholarship, NSFC Funding). **Andrzej I. Stankiewicz:** Writing - review & editing, Funding acquisation (ADREM), Supervision. **Farnaz Eghbal Sarabi:** Writing - review & editing. **Hakan Nigar:** Writing - review & editing, Supervision.

Declaration of Competing Interest

The authors declare that they have no known competing financial interests or personal relationships that could have appeared to influence the work reported in this paper.

Acknowledgements

Financial support from the European Union's Horizon 2020 research and innovation programme ADREM (No. 680777) is gratefully acknowledged. Peng Yan acknowledges the financial support from China Scholarship Council (No. 201706250076) for his joint PhD research with Prof. Andrzej I. Stankiewicz at the Delft University of Technology, The Netherlands. Peng Yan acknowledges the financial support from the National Natural Science Foundation of China (No. 22008137). Many thanks to Dr. Guido S. J. Sturm for the helpful discussion on the fundamentals of microwave engineering.

Appendix A. Supplementary material

Supplementary data to this article can be found online at https://doi.org/10.1016/j.ces.2020.116383.

References

Barham, J.P., Koyama, E., Norikane, Y., Ohneda, N., Yoshimura, T., 2019. Microwave Flow: A Perspective on Reactor and Microwave Configurations and the Emergence of Tunable Single-Mode Heating Toward Large-Scale Applications. Chem. Rec. 19, 188–203.

Bermúdez, J.M., Beneroso, D., Rey-Raap, N., Arenillas, A., Menéndez, J.A., 2015. Energy consumption estimation in the scaling-up of microwave heating processes. Chem. Eng. Process. 95, 1–8.

Bird, R.B., Stewart, W.E., Lightfoot, E.N., 2002. Transport Phenomena. John Wiley & Sons, New York.

COMSOL, 2017a. CFD Module User's Guide. COMSOL Multiphysics® v. 5.3. www.comsol.com. COMSOL AB, Stockholm, Sweden.

COMSOL, 2017b. Heat Transfer Module User's Guide. COMSOL Multiphysics® v. 5.3. www.comsol.com. COMSOL AB, Stockholm, Sweden.

COMSOL, 2017c. RF Module User's Guide. COMSOL Multiphysics® v. 5.3. www.comsol.com. COMSOL AB, Stockholm, Sweden.

Eghbal Sarabi, F., Ghorbani, M., Stankiewicz, A., Nigar, H., 2020. Coaxial traveling-wave microwave reactors: Design challenges and solutions. Chem. Eng. Res. Des. 153, 677–683.

Franssen, I.S., Irimia, D., Stefanidis, G.D., Stankiewicz, A.I., 2014. Practical challenges in the energy-based control of molecular transformations in chemical reactors. AIChE J. 60, 3392–3405.

Gangurde, L.S., Sturm, G.S.J., Devadiga, T.J., Stankiewicz, A.I., Stefanidis, G.D., 2017. Complexity and Challenges in Noncontact High Temperature Measurements in Microwave-Assisted Catalytic Reactors. Ind. Eng. Chem. Res. 56, 13379–13391.

Gao, X., Liu, X., Yan, P., Li, X., Li, H., 2019. Numerical analysis and optimization of the microwave inductive heating performance of water film. Int. J. Heat Mass. Tran 139, 17–30.

Haneishi, N., Tsubaki, S., Abe, E., Maitani, M.M., Suzuki, E.-I., Fujii, S., Fukushima, J., Takizawa, H., Wada, Y., 2019. Enhancement of Fixed-bed Flow Reactions under Microwave Irradiation by Local Heating at the Vicinal Contact Points of Catalyst Particles. Sci. Rep. 9, 222.

Horikoshi, S., Serpone, N., 2014. Role of microwaves in heterogeneous catalytic systems. Catal. Sci. Technol. 4, 1197–1210.

Julian, I., Ramirez, H., Hueso, J.L., Mallada, R., Santamaria, J., 2019. Non-oxidative methane conversion in microwave-assisted structured reactors. Chem. Eng. J. 377, 119764.

Mitani, T., Hasegawa, N., Nakajima, R., Shinohara, N., Nozaki, Y., Chikata, T., Watanabe, T., 2016. Development of a wideband microwave reactor with a coaxial cable structure. Chem. Eng. J. 299, 209–216.

Muley, P.D., Henkel, C.E., Aguilar, G., Klasson, K.T., Boldor, D., 2016. Ex situ thermo-catalytic upgrading of biomass pyrolysis vapors using a traveling wave microwave reactor. Appl. Energ. 183, 995–1004.
Nield, D.A., Bejan, A., 2017. Convection in Porous Media. Springer, New York.
Nigar, H., Navascués, N., de la Iglesia, O., Mallada, R., Santamaría, J., 2015. Removal of VOCs at trace concentration levels from humid air by Microwave Swing Adsorption, kinetics and proper sorbent selection. Sep. Purif. Technol. 151, 193–200.
Nigar, H., Sturm, G.S.J., Garcia-Baños, B., Peñaranda-Foix, F.L., Catalá-Civera, J.M., Mallada, R., Stankiewicz, A., Santamaría, J., 2019. Numerical analysis of microwave heating cavity: Combining electromagnetic energy, heat transfer and fluid dynamics for a NaY zeolite fixed-bed. Appl. Therm. Eng. 155, 226–238.
Nishioka, M., Miyakawa, M., Daino, Y., Kataoka, H., Koda, H., Sato, K., Suzuki, T.M., 2013. Single-Mode Microwave Reactor Used for Continuous Flow Reactions under Elevated Pressure. Ind. Eng. Chem. Res. 52, 4683–4687.
Oliver Kappe, C., 2008. Microwave dielectric heating in synthetic organic chemistry. Chem. Soc. Rev. 37, 1127–1139.
Polaert, I., Estel, L., Delmotte, M., Luart, D., Len, C., 2017. A new and original microwave continuous reactor under high pressure for future chemistry. AIChE J. 63, 192–199.
Pozar, D., 2012a. Chapter 3 Transmission lines and Waveguides, Microwave Engineering. John Wiley & Sons.
Pozar, D., 2012b. Microwave Engineering. John Wiley & Sons.
Ramirez, A., Hueso, J.L., Abian, M., Alzueta, M.U., Mallada, R., Santamaria, J., 2019. Escaping undesired gas-phase chemistry: Microwave-driven selectivity enhancement in heterogeneous catalytic reactors. Sci. Adv. 5, eaau9000.
Ramirez, A., Hueso, J.L., Mallada, R., Santamaria, J., 2020. Microwave-activated structured reactors to maximize propylene selectivity in the oxidative dehydrogenation of propane. Chem. Eng. J. 393, 124746.
Satterfield, C.N., 1996. Heterogeneous catalysis in Industrial practice. McGraw-Hill, New York.
Stankiewicz, A., 2006. Energy Matters: Alternative Sources and Forms of Energy for Intensification of Chemical and Biochemical Processes. Chem. Eng. Res. Des. 84, 511–521.
Stankiewicz, A., Sarabi, F.E., Baubaid, A., Yan, P., Nigar, H., 2019. Perspectives of Microwaves-Enhanced Heterogeneous Catalytic Gas-Phase Processes in Flow Systems. Chem. Rec. 19, 40–50.
Stefanidis, G.D., Navarrete, M.A., Sturm, G.S.J., Stankiewicz, A.I., 2014. A Helicopter View of Microwave Application to Chemical Processes: Reactions, Separations, and Equipment Concepts. Rev. Chem. Eng. 46, 233–259.
Sturm, G.S.J., Stankiewicz, A.I., Stefanidis, G.D., 2016. CHAPTER 4 Microwave Reactor Concepts: From Resonant Cavities to Traveling Fields, Alternative Energy Sources for Green Chemistry. Royal Soc. Chem., 93–125
Sturm, G.S.J., Verweij, M.D., Stankiewicz, A.I., Stefanidis, G.D., 2014. Microwaves and microreactors: Design challenges and remedies. Chem. Eng. J. 243, 147–158.
Sturm, G.S.J., Verweij, M.D., van Gerven, T., Stankiewicz, A.I., Stefanidis, G.D., 2012. On the effect of resonant microwave fields on temperature distribution in time and space. Int. J. Heat Mass. Tran. 55, 3800–3811.
Sturm, G.S.J., Verweij, M.D., van Gerven, T., Stankiewicz, A.I., Stefanidis, G.D., 2013. On the parametric sensitivity of heat generation by resonant microwave fields in process fluids. Int. J. Heat Mass. Tran. 57, 375–388.
Wakao, N., 1976. Particle-to-fluid transfer coefficients and fluid diffusivities at low flow rate in packed beds. Chem. Eng. Sci. 31, 1115–1122.
Wakao, N., Kaguei, S., Funazkri, T., 1979. Effect of fluid dispersion coefficients on particle-to-fluid heat transfer coefficients in packed beds: Correlation of nusselt numbers. Chem. Eng. Sci. 34, 325–336.